Hindawi Publishing Corporation
Mathematical Problems in Engineering
Volume 2009, Article ID 471804, 36 pages
doi:10.1155/2009/471804

Research Article

Internal Loading Distribution in Statically Loaded Ball Bearings Subjected to an Eccentric Thrust Load

Mário César Ricci

Space Mechanics and Control Division (DMC), Brazilian Institute for Space Research (INPE), São José dos Campos 12227-010, Brazil

Correspondence should be addressed to Mário César Ricci, mariocesarricci@uol.com.br

Received 29 July 2009; Accepted 18 November 2009

Recommended by Antonio Prado

Rolling-element bearings are simple machine elements of great utility used both in simple commercial devices as in complex engineering mechanisms. Because of being a very popular machine element, there is a lot of literature on the subject. With regard to the behavior of internal loading distribution, elastic deformations at point or line contacts, and geometric parameters under loading, although there are many works describing the parameters variation models, few works show such variations in practice, even under simple static loadings. In an attempt to cover this gap some studies are being developed in parallel. Particularly in this work, a *new*, iterative computational procedure is introduced which calculates internal normal ball loads in statically loaded single-row, angular-contact ball bearings, subjected to a known thrust load which is applied to a variable distance (lever arm or eccentricity) from the geometric bearing center line. Numerical examples results for a 218 angular-contact ball bearing have been compared with those from the literature. Fifty figures are presented showing geometrical features and the following parameters variations as functions of the thrust load and eccentricity: contact angle, contact ellipse parameters, normal ball loads, distances between groove curvature centers, normal and axial deflections, and loading zones.

1. Introduction

Ball and roller bearings, generically called *rolling bearings*, are commonly used machine elements. They are employed to permit rotary motions of, or about, shafts in simple commercial devices such as bicycles, roller skates, and electric motors. They are also used in complex engineering mechanisms such as aircraft gas turbines, rolling mils, dental drills, gyroscopes, and power transmissions.

The standardized forms of ball or roller bearings permit rotary motion between two machine elements and always include a complement of ball or rollers that maintain the shaft and a usually stationary supporting structure, frequently called a *housing*, in a radially or axially spaced-apart relationship. Usually, a bearing may be obtained as a unit, which

Figure 1: An angular-contact ball bearing (courtesy of SKF Industries).

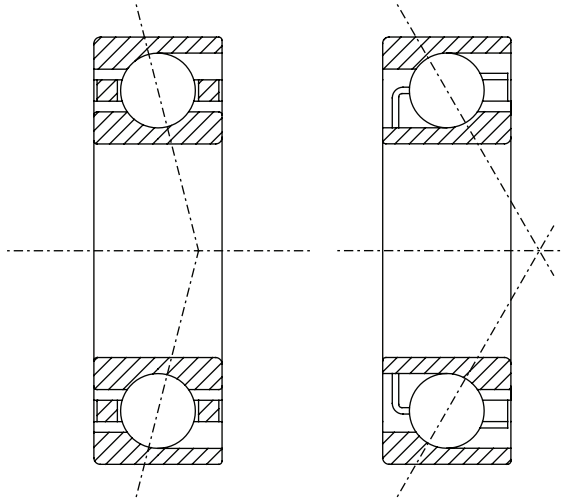

(a) Small angle (b) Large angle

Figure 2: Angular-contact ball bearings.

includes two steel rings; each of which has a hardened raceway on which hardened balls or rollers roll. The balls or rollers, also called *rolling elements*, are usually held in an angularly spaced relationship by a *cage*, also called a *separator* or *retainer*.

There are many different kinds of rolling bearings. This work is concerned with *single-row angular-contact ball bearings* (Figure 1) that are designed to support combined radial and thrust loads or heavy thrust loads depending on the contact angle magnitude. The bearings having large contact angle can support heavier thrust loads. Figure 2 shows bearings having small and large contact angles. The bearings generally have groove curvature radii in the range of 52%–53% of the ball diameter. The contact angle does not usually exceed 40^o.

This work is devoted to the study of the internal loading distribution in statically loaded ball bearings. Several researchers have studied the subject as, for example, Stribeck [1], Sjoväll [2], Jones [3], and Rumbarger [4], to cite a few. The methods developed by

them to calculate distribution of load among the balls and rollers of rolling bearings can be used in most bearing applications because rotational speeds are usually slow to moderate. Under these speed conditions, the effects of rolling-element centrifugal forces and gyroscopic moments are negligible. At high speeds of rotation these body forces become significant, tending to alter contact angles and clearance. Thus, they can affect the static load distribution to a great extension.

Harris [5] described methods for internal loading distribution in statically loaded bearings addressing pure radial, pure thrust (centric and eccentric loads), combined radial and thrust load, which uses radial and thrust integrals introduced by Sjoväll [2], and for ball bearings under combined radial, thrust, and moment load, initially due to Jones [3].

The method described by Harris for eccentric thrust load, initially due to Rumbarger [4], is an approximate, direct method, based in a single-row, 90^o thrust bearing and in thrust and moment integrals whose values are obtained from tables and graphics, as functions of eccentricity and pitch diameter. The maximum ball load is given directly and no computer is necessary. Although it is not entirely appropriate, the method was used by Harris to find approximations for the maximum ball load magnitude and for the extension of the loading zone in the 218 angular-contact ball bearing.

We can see that there are many works describing the parameters variation models under static loads but few show such variations in practice, even under simple static loadings. The author believes that the lack of practical examples in the literature is mainly due to the inherent difficulties of the numerical procedures that, in general, deal with the resolution of several nonlinear algebraic equations that must be solved simultaneously.

In an attempt to cover this gap studies are being developed in parallel [6–14]. Particularly in this work is described a new, precise method for internal load distribution computation in statically loaded, single-row, angular-contact ball bearings subjected to a known external thrust load which is applied to a variable distance (lever arm or eccentricity) from the geometric bearing center line. It must be solved iteratively using a digital computer and can be thought as a particular case of the Jones method, with null external radial load and external moment load given by the product of the thrust load by the eccentricity. Unlike Rumbarger's method, it is adequate to angular-contact bearings, and theoretically and numerically more precise. The novelty of the method is in the choice of the set of the nonlinear equations, which must be solved simultaneously. The author did not find in the literature the resolution of this problem using the same set of equations.

The difference between the method described here and the method described by Harris for eccentric thrust load mainly comes from the fact that Rumbarger's method, for sake of simplicity, makes use of the pitch radius, $d_e/2$, as lever arm, instead of the inner contact radius, $d_{cj}/2$, in the r.h.s. of the moment equation—see (4.19) for comparison— and secondarily by the fact that it uses the pitch radius instead of the locus of the centers of the inner ring raceway groove curvature radii, R_i, in the computations of the load distribution factor, ε, in (4.10) and of the extension of load zone, φ_l, in (4.11). These approximations are guarantee of the straightforwardness but obviously they introduce errors in the normal ball loads determination. However, at first glance appears that the method for thrust bearing is more attractive than the method of this paper because it supplies results more directly whereas no computer is necessary. But, despite the simplicity of the former, comparative analyses between the results show significant differences in the magnitudes of the maximum ball load and extension of the loading zone.

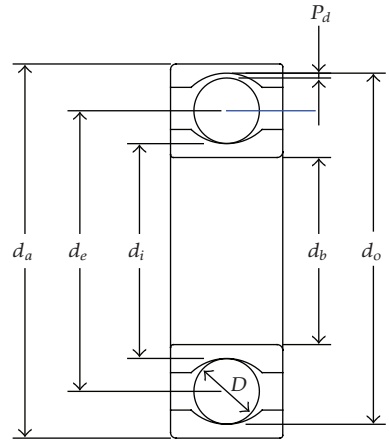

Figure 3: Radial cross-section of a single-row ball bearing.

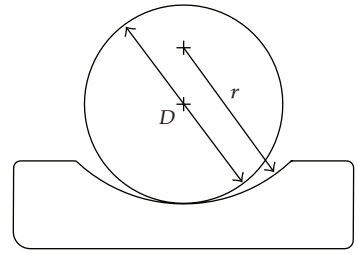

Figure 4: Cross-section of a ball and an outer race showing race conformity.

2. Geometry of Ball Bearings

In this section, the principal geometrical relationships for an unloaded ball bearing are summarized. The radial cross section of a single-row ball bearing shown in Figure 3 depicts the *diametral clearance* and various diameters. The *pitch diameter*, d_e, is the mean of the inner- and outer-race diameters d_i and d_o, respectively, and is given by

$$d_e = \frac{1}{2}(d_i + d_o). \tag{2.1}$$

The diametral clearance, P_d, can be written as

$$P_d = d_o - d_i - 2D. \tag{2.2}$$

Race conformity is a measure of the geometrical conformity of the race and the ball in a plane passing through the bearing axis (also named center line or rotation axis), which is a line passing through the center of the bearing perpendicular to its plane and transverse to the race. Figure 4 depicts a cross section of a ball bearing showing race conformity expressed as

$$f = \frac{r}{D}. \tag{2.3}$$

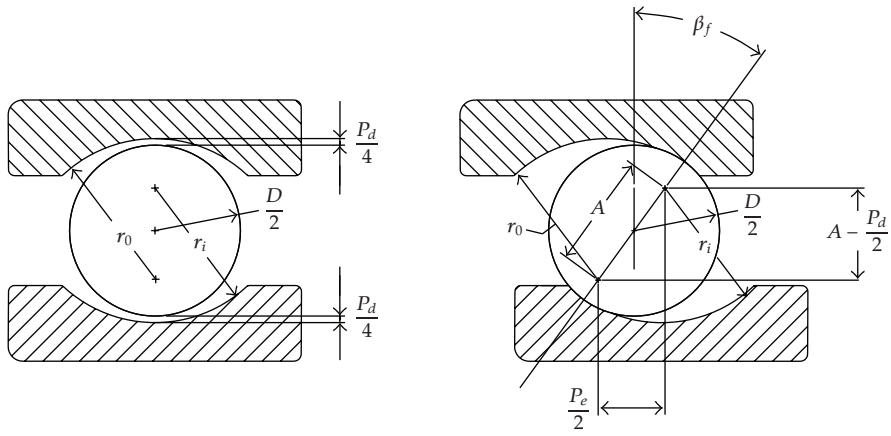

(a) Initial position

(b) Shifted position

Figure 5: Cross-section of a radial ball bearing showing ball-race contact due to axial shift of inner and outer rings.

Radial bearings have some axial play since they are generally designed to have a diametral clearance, as shown in Figures 5(a) and 5(b), that shows a radial bearing with contact due to the axial shift of the inner and outer rings when no measurable force is applied. The radial distances between the curvature centers of the two races are the same in Figures 5(a) and 5(b). Denoting quantities which referred to the inner and outer races by subscripts i and o, respectively, this radial distance value can be expressed as $A - P_d/2$, where $A = r_o + r_i - D$ is the curvature centers distance in the shifted position given by Figure 5(b). Using (2.3) we can write A as

$$A = BD, \tag{2.4}$$

where $B = f_o + f_i - 1$ is known as the *total conformity ratio* and is a measure of the combined conformity of both the outer and inner races to the ball.

The *contact angle*, β, is defined as the angle made by a line, which passes through the curvature centers of both the outer and inner raceways and that lies in a plane passing through the bearing rotation axis, with a plane perpendicular to the bearing axis of rotation. The *free-contact angle*, β_f, (Figure 5(b)) is the contact angle when the line also passes through the points of contact of the ball and both raceways and no measurable force is applied. From Figure 5(b), the expression for the free-contact angle can be written as

$$\cos\beta_f = \frac{A - P_d/2}{A}. \tag{2.5}$$

From (2.5), the diametral clearance, P_d, can be written as

$$P_d = 2A\left(1 - \cos\beta_f\right). \tag{2.6}$$

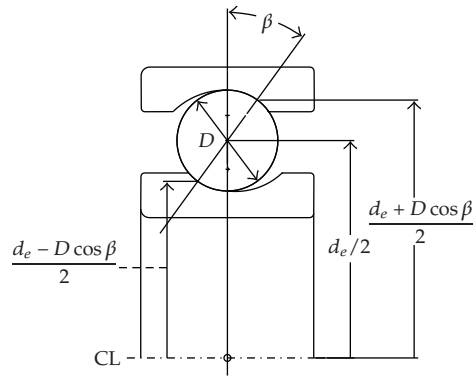

Figure 6: Cross-section of a ball bearing.

Free endplay, P_e, is the maximum axial movement of the inner race with respect to the outer when both races are coaxially centered and no measurable force is applied. Free endplay depends on total curvature and contact angle, as shown in Figure 5(b), and can be written as

$$P_e = 2A \sin \beta_f. \tag{2.7}$$

Considering the geometry of two contacting solids (ellipsoids) in a ball bearing, we can arrive at the two quantities of some importance in the analysis of contact stresses and deformations. The curvature sum, $1/R$, and curvature difference, Γ, are defined as

$$\begin{aligned} \frac{1}{R} &= \frac{1}{R_x} + \frac{1}{R_y}, \\ \Gamma &= R\left(\frac{1}{R_x} - \frac{1}{R_y}\right), \end{aligned} \tag{2.8}$$

where

$$\begin{aligned} \frac{1}{R_x} &= \frac{1}{r_{ax}} + \frac{1}{r_{bx}}, \\ \frac{1}{R_y} &= \frac{1}{r_{ay}} + \frac{1}{r_{by}}, \end{aligned} \tag{2.9}$$

with r_{ax}, r_{bx}, r_{ay}, and r_{by} being the radii of curvature for the ball-race contact.

A cross section of a ball bearing operating at a contact angle β is shown in Figure 6. Equivalent radii of curvature for both inner- and outer-race contacts in, and normal to, the direction of rolling can be calculated from this figure. Considering x the direction of the

motion and y the transverse direction, the radii of curvature for the ball-inner-race contact are

$$\begin{aligned} r_{ax} &= r_{ay} = \frac{D}{2}, \\ r_{bx} &= \frac{d_e - D\cos\beta}{2\cos\beta}, \\ r_{by} &= -f_i D = -r_i. \end{aligned} \tag{2.10}$$

The radii of curvature for the ball-outer-race contact are

$$\begin{aligned} r_{ax} &= r_{ay} = \frac{D}{2}, \\ r_{bx} &= -\frac{d_e + D\cos\beta}{2\cos\beta}, \\ r_{by} &= -f_o D = -r_o. \end{aligned} \tag{2.11}$$

Let

$$\gamma = \frac{D\cos\beta}{d_e}. \tag{2.12}$$

Then

$$\begin{aligned} r_{bx} &= \frac{D}{2}\frac{1-\gamma}{\gamma}, \\ \left.\frac{1}{R}\right|_i &= \frac{1}{r_{ax}} + \frac{1}{r_{bx}} + \frac{1}{r_{ay}} + \frac{1}{r_{by}} = \frac{1}{D}\left(4 - \frac{1}{f_i} + \frac{2\gamma}{(1-\gamma)}\right), \\ \Gamma_i &= R\left(\frac{1}{r_{ax}} + \frac{1}{r_{bx}} - \frac{1}{r_{ay}} - \frac{1}{r_{by}}\right) = \frac{1/f_i + 2\gamma/(1-\gamma)}{4 - 1/f_i + 2\gamma/(1-\gamma)}, \end{aligned} \tag{2.13}$$

for the ball-inner-race contact, and

$$\begin{aligned} r_{bx} &= -\frac{D}{2}\frac{1+\gamma}{\gamma}, \\ \left.\frac{1}{R}\right|_o &= \frac{1}{r_{ax}} + \frac{1}{r_{bx}} + \frac{1}{r_{ay}} + \frac{1}{r_{by}} = \frac{1}{D}\left(4 - \frac{1}{f_o} - \frac{2\gamma}{1+\gamma}\right), \\ \Gamma_o &= R\left(\frac{1}{r_{ax}} + \frac{1}{r_{bx}} - \frac{1}{r_{ay}} - \frac{1}{r_{by}}\right) = \frac{1/f_o\ - 2\gamma/(1+\gamma)}{4 - 1/f_o - 2\gamma/(1+\gamma)}, \end{aligned} \tag{2.14}$$

for the ball-outer-race contact.

3. Contact Stress and Deformations

When two elastic solids are brought together under a load, a contact area develops; the shape and size of which depend on the applied load, the elastic properties of the materials, and the curvatures of the surfaces. For two ellipsoids in contact the shape of the contact area is elliptical, with a being the semimajor axis in the y direction (transverse direction) and b being the semiminor axis in the x direction (direction of motion).

The *elliptical eccentricity parameter*, k, is defined as

$$k = \frac{a}{b}. \tag{3.1}$$

From Harris [5], k can be written in terms of the curvature difference, Γ, and the *elliptical integrals of the first and second kind*s $\mathbf{K}$ and $\mathbf{E}$, as

$$J(k) = \sqrt{\frac{2\mathbf{K} - \mathbf{E}(1+\Gamma)}{\mathbf{E}(1-\Gamma)}}, \tag{3.2}$$

where

$$\begin{aligned} \mathbf{K} &= \int_0^{\pi/2} \left[1 - \left(1 - \frac{1}{k^2}\right)\sin^2\varphi\right]^{-1/2} d\varphi, \\ \mathbf{E} &= \int_0^{\pi/2} \left[1 - \left(1 - \frac{1}{k^2}\right)\sin^2\varphi\right]^{1/2} d\varphi. \end{aligned} \tag{3.3}$$

A one-point iteration method which has been used successfully in the past [15] is used, where

$$k_{n+1} = J(k_n). \tag{3.4}$$

When the *ellipticity parameter*, k, the *elliptic integrals of the first* and *second kinds*, $\mathbf{K}$ and $\mathbf{E}$, respectively, the normal applied load, Q, Poisson's ratio, ν, and the modulus of elasticity, E, of the contacting solids, are known, we can write the semimajor and semiminor axes of the contact ellipse and the maximum deformation at the center of the contact, from the analysis of Hertz [16], as

$$\begin{aligned} a &= \left(\frac{6k^2\mathbf{E}QR}{\pi E'}\right)^{1/3}, \\ b &= \left(\frac{6\mathbf{E}QR}{\pi k E'}\right)^{1/3}, \end{aligned} \tag{3.5}$$

$$\delta = \mathbf{K}\left[\frac{9}{2\mathbf{E}R}\left(\frac{Q}{\pi k E'}\right)^2\right]^{1/3}, \tag{3.6}$$

where

$$E' = \frac{2}{(1-\upsilon_a^2)/E_a + (1-\upsilon_b^2)/E_b}. \tag{3.7}$$

4. Static Load Distribution under Eccentric Thrust Load

Methods to calculate distribution of load among the balls and rollers of rolling bearings statically loaded can be found in various papers [5, 17]. The methods have been limited to, at most, three degrees of freedom in loading and demand the solution of a simultaneous nonlinear system of algebraic equations for higher degrees of freedom. Solution of such equations generally necessitates the use of a digital computer. In certain cases, however—for example, applications with pure radial, pure thrust, or radial and thrust loading with nominal clearance—the simplified methods will probably provide sufficiently accurate calculational results.

Having defined a simple analytical expression for the deformation in terms of load in the previous section, it is possible to consider how the bearing load is distributed among the rolling elements. Most rolling-element bearing applications involve steady-state rotation of either the inner or outer race or both; however, the speeds of rotation are usually not so great as to cause ball or roller centrifugal forces or gyroscopic moments of significant magnitudes. In analyzing the loading distribution on the rolling elements, it is usually satisfactory to ignore these effects in most applications. In this section the load-deflection relationships for ball bearings are given, along with a specific load distribution consisting of an eccentric thrust load of statically loaded rolling elements.

4.1. Load-Deflection Relationships for Ball Bearings

From (3.6) it can be seen that for a given ball-raceway contact (point loading)

$$Q = K\delta^{3/2}, \tag{4.1}$$

where

$$K = \pi k E' \sqrt{\frac{2\mathbf{E}R}{9\mathbf{K}^3}}. \tag{4.2}$$

The total normal approach between two raceways under load separated by a rolling element is the sum of the approaches between the rolling element and each raceway. Hence

$$\delta_n = \delta_i + \delta_o. \tag{4.3}$$

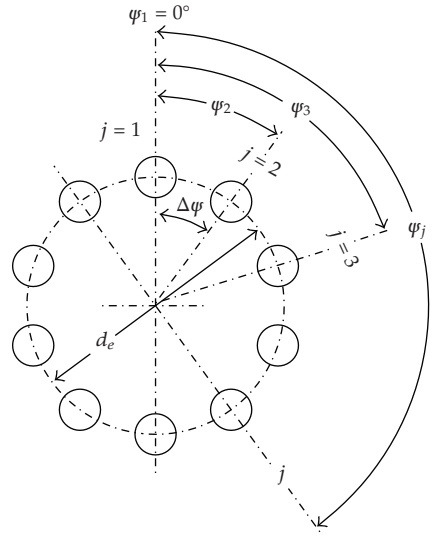

Figure 7: Ball angular positions in the radial plane that is perpendicular to the bearing's axis of rotation; $\Delta\psi = 2\pi/Z, \psi_j = 2\pi/Z(j-1)$.

Therefore,

$$K_n = \left[\frac{1}{1/{K_i}^{2/3} + 1/{K_o}^{2/3}}\right]^{3/2}, \tag{4.4}$$

$$Q = K_n \delta_n^{3/2}. \tag{4.5}$$

4.2. Ball Bearings under Eccentric Thrust Load

Let a ball bearing with a number of balls, Z, symmetrically distributed about a pitch circle according to Figure 7, be subjected to an eccentric thrust load. Then, a *relative axial displacement*, δ_a, and a *relative angular displacement*, θ, between the inner and outer ring raceways may be expected. Let $\psi = 0$ be the angular position of the maximum loaded ball.

Figure 8 shows the initial and final curvature centers positions at angular position ψ, before and after loading, whereas the centers of curvature of the raceway grooves are fixed with respect to the corresponding raceway. If δ_a and θ are known, then the *total axial displacement*, δ_t, at angular position ψ, is given by

$$\delta_t(\psi) = \delta_a + R_i \theta \cos\psi, \tag{4.6}$$

where

$$R_i = \frac{d_e}{2} + (f_i - 0.5) D \cos\beta_f \tag{4.7}$$

expresses the locus of the centers of the inner ring raceway groove curvature radii.

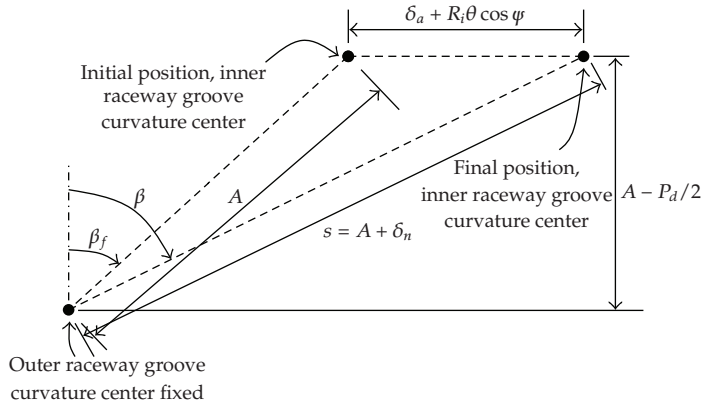

Figure 8: Initial and final curvature centers positions at angular position ψ, with and without applied load.

Also,

$$\delta_{\max} \equiv \delta_t(0) = \delta_a + R_i\theta. \tag{4.8}$$

From (4.6) and (4.8), one may develop the following relationship:

$$\delta_t = \delta_{\max}\left[1 - \frac{1}{2\varepsilon}(1 - \cos\psi)\right] \tag{4.9}$$

in which

$$\varepsilon = \frac{1}{2}\left(1 + \frac{\delta_a}{R_i\theta}\right). \tag{4.10}$$

The extension of the *loading zone* is defined by

$$\psi_l = \cos^{-1}\left(\frac{-\delta_a}{R_i\theta}\right). \tag{4.11}$$

From Figure 8,

$$\beta(\psi) = \cos^{-1}\left(\frac{A - P_d/2}{A + \delta_n}\right), \tag{4.12}$$

$$\delta_t(\psi) = (A + \delta_n)\sin\beta - A\sin\beta_f. \tag{4.13}$$

From (2.5) and (4.12), the total normal approach between two raceways at angular position ψ, after the thrust load has been applied, can be written as

$$\delta_n(\psi) = A\left(\frac{\cos\beta_f}{\cos\beta} - 1\right). \tag{4.14}$$

From Figure 8 and (4.14) it can be determined that s, the distance between the centers of the curvature of the inner and outer ring raceway grooves at any rolling-element position ψ, is given by

$$s(\psi) = A + \delta_n = A\frac{\cos\beta_f}{\cos\beta}. \tag{4.15}$$

From (4.6), (4.13), and (4.14), yields, for $\psi = \psi_j$,

$$\delta_a + R_i\theta\cos\psi_j - A\frac{\sin(\beta_j - \beta_f)}{\cos\beta_j} = 0, \quad j = 1,\ldots,Z. \tag{4.16}$$

From (4.5), and (4.14) one yields, for $\psi = \psi j$,

$$Q_j = K_{nj}A^{3/2}\left(\frac{\cos\beta_f}{\cos\beta_j} - 1\right)^{3/2}, \quad j = 1,\ldots,Z. \tag{4.17}$$

If the external thrust load, F_a, is applied at a point distant e from the bearing's axis of rotation, then for static equilibrium to exist

$$F_a = \sum_{j=1}^{Z} Q_j\sin\beta_j, \tag{4.18}$$

$$M = eF_a = \frac{1}{2}\sum_{j=1}^{Z} d_{cj}Q_j\sin\beta_j\cos\psi_j, \tag{4.19}$$

where $d_{cj} \equiv d_e - D\cos\beta_j$.

Substitution of (4.17) into (4.18) yields

$$F_a - A^{3/2}\sum_{j=1}^{Z} K_{nj}\sin\beta_j\left(\frac{\cos\beta_f}{\cos\beta_j} - 1\right)^{3/2} = 0. \tag{4.20}$$

Similarly,

$$eF_a - \frac{A^{3/2}}{2}\sum_{j=1}^{Z} K_{nj}d_{cj}\cos\psi_j\sin\beta_j\left(\frac{\cos\beta_f}{\cos\beta_j} - 1\right)^{3/2} = 0. \tag{4.21}$$

Equations (4.16), (4.20), and (4.21) are $Z + 2$ simultaneous nonlinear equations with unknowns δ_a, θ, and β_j, $j = 1,\ldots,Z$. Since K_{nj} and d_{cj} are functions of final contact angle, β_j, the equations must be solved iteratively to yield an exact solution for δ_a, θ, and β_j.

5. Numerical Results

A numerical method (the Newton-Rhapson method) was chosen to solve the simultaneous nonlinear equations (4.16), (4.20), and (4.21). Choosing the rolling bearing, input must be given the geometric parameters d_i, d_o, D, Z, r_i, and r_o, in accordance with Figures 3 and 5, and the elastic properties E_a, E_b, ν_a, and ν_b. Next, the following parameters must be obtained: f_i, f_o, B, A, $\psi_j (j = 1, \ldots, Z)$, E', d_e, P_d, β_f, and R_i.

The interest here is to observe the behavior of an angular-contact ball bearing under a known thrust load which is to be applied statically to a *variable* distance (lever arm or eccentricity), e, from the geometric bearing center line. Then, given a thrust load and the initial estimates for δ_a, θ, and β_j, $j = 1, \ldots, Z$, for each distance e, varying from zero up to a given maximum eccentricity, the values $1/R|_i$, $1/R|_o$, Γ_i, Γ_o, k_i, k_o, $\mathbf{K}_i$, $\mathbf{K}_o$, $\mathbf{E}_i$, $\mathbf{E}_o$, K_i, K_o, and K_n are calculated for each ball, according to previous sections, and new values for δ_a, θ, and β_j are obtained. The new β_j values are compared with old ones, and if the difference is greater than a minimal error, then new values for $1/R|_i$, $1/R|_o$, Γ_i, Γ_o, k_i, k_o, $\mathbf{K}_i$, $\mathbf{K}_o$, $\mathbf{E}_i$, $\mathbf{E}_o$, K_i, K_o, and K_n are calculated for each ball, and again new values for δ_a, θ, and β_j are obtained. If the difference is lesser than the error then a new value for e is taken. If e is the last valid value, then a new thrust load value is acquired and the procedure is repeated up to the last valid thrust load value, when the program ends.

To show an application of the theory developed in this work, a numerical example is presented here. It was chosen the 218 angular-contact ball bearing that was also used by Harris[5]. Thus, the results generated here can be compared to a certain degree with Harris results. The input data for this rolling bearing were the following:

inner raceway diameter: $d_i = 0.10279\,\text{m}$,
outer raceway diameter: $d_o = 0.14773\,\text{m}$,
ball diameter: $D = 0.02223\,\text{m}$,
ball number: $Z = 16$,
inner groove radius: $r_i = 0.01163\,\text{m}$,
outer groove radius: $r_o = 0.01163\,\text{m}$,
modulus of elasticity for both balls and races: $E = 2.075 \times 10^{11}\,\text{N/m}^2$,
poisson's ratio for both balls and races: $\upsilon = 0.3$.

The remaining parameters have been calculated yielding:

inner race conformity: $f_i = 0.523166891587944$,
outer race conformity: $f_o = 0.523166891587944$,
total conformity ratio: $B = 0.046333783175888$,
initial curvature centers distance: A=0.00103 m,
effective elastic modulus: $E' = 228021978021.978\,\text{N/m}^2$,
angular spacing between rolling elements: $\Delta\psi = 22.5°$,
angular position of rolling elements: $\psi_j = 22.5°(j - 1)$, $j = 1, \ldots, 16$,
bearing pitch diameter: $d_e = 0.12526\,\text{m}$,
diametral clearance: $P_d = 0.00048\,\text{m}$,
free-contact angle: $\beta_f = 39.915616407992260°$,
radius of locus of inner raceway groove curvature centers: $R_i = 0.063025\,\text{m}$.

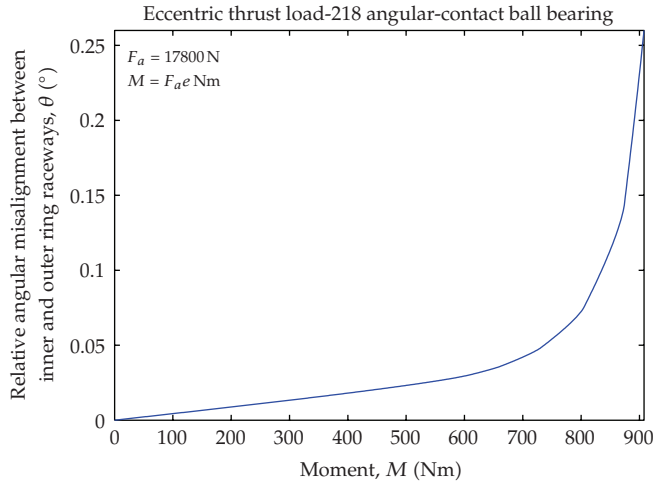

Figure 9: Relative angular misalignment, θ, for 17,800 N thrust load, as a function of the Moment, M.

For each thrust load value, the initial estimates for δ_a, θ, and β_j were the following:

axial deflection: $\delta^a = 10^{-5}$ m,

misalignment angle: $\theta = 10^{-2}$ rd,

contact angle: $\beta_j = 1.1\beta_f$, $j = 1, \ldots, 16$.

5.1. Numerical Results for a 17,800 N Thrust Load

Since it is the qualitative behavior of solutions that is the interest, the results are presented here in graphical form.

Initially, for comparative purposes with the Harris work, a specific thrust load $F_a = 17,800$ N was chosen to be applied, and the following graphical results are presented as functions of the moment, $M = F_a e$:

(i) relative angular displacement, θ (Figure 9),

(ii) partial axial displacement, $R_i\theta\cos\psi$ (Figure 10),

(iii) relative axial displacement, δ_a (Figure 11),

(iv) total relative axial deflection, δ_t (Figure 12),

(v) loading zone, ψ_l (Figure 13),

(vi) distance between loci of inner and outer raceway groove curvature centers, s (Figure 14),

(vii) maximum elastic compression at the ball/inner-race contact, δ_i (Figure 15),

(viii) maximum elastic compression at the ball/outer-race contact, δ_o (Figure 16),

(ix) total normal ball deflection, δ_n (Figure 17),

(x) ball-raceway normal load, Q (Figure 18),

(xi) contact angle, β (Figure 19),

(xii) semimajor axis of the ball/inner-race contact area, a_i (Figure 20),

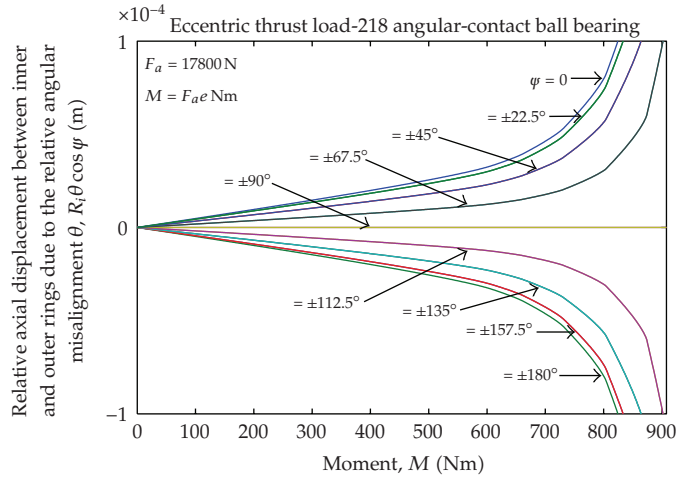

Figure 10: Partial axial deflection, $R_i\theta\cos\psi$, for each ball and 17,800 N thrust load, as a function of the Moment, M.

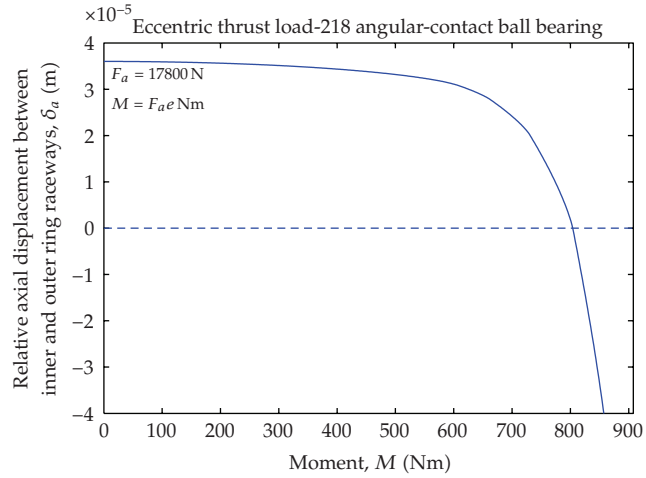

Figure 11: Axial deflection, δ_a, for 17,800 N thrust load, as a function of the Moment, M.

(xiii) semiminor axis of the ball/inner-race contact area, b_i (Figure 21),

(xiv) semimajor axis of the ball/outer-race contact area, a_o (Figure 22),

(xv) semiminor axis of the ball/outer-race contact area, b_o (Figure 23),

(xvi) elliptical eccentricity parameter for ball/inner-race contact, k_i (Figure 24),

(xvii) elliptical eccentricity parameter for ball/outer-race contact, k_o (Figure 25).

The graphics above, with exception of Figures 9, 11, and 13, show one curve for each ball angular position.

Figures 9 and 10 show the relative angular misalignment, θ, and the partial axial deflection for each ball, $R_i\theta\cos\psi$, respectively. It is observed that there is an approximately linear relationship between the misalignment angle, θ, and applied moment, M, for moment

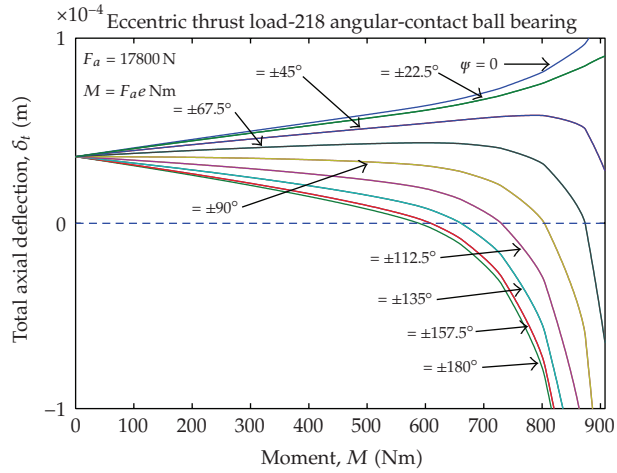

Figure 12: Total axial deflection, δ_t, for 17,800 N thrust load, as a function of the Moment, M.

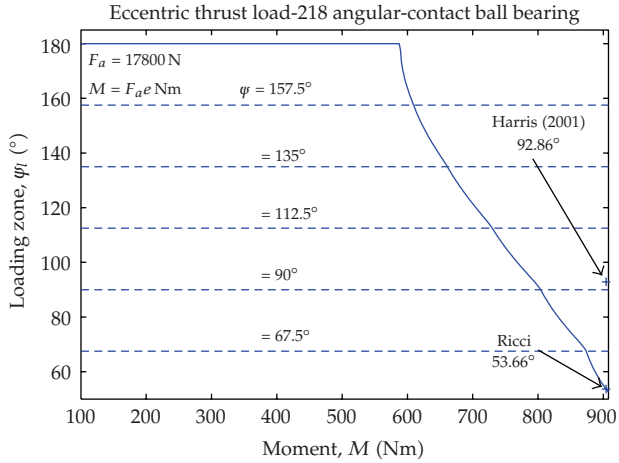

Figure 13: Loading zone, ψ_l, for 17,800 N thrust load, as a function of the Moment, M.

values ranging from zero up to about 600 Nm, which corresponds to a distance e of approximately 33.7 mm. Keeping the load constant and increasing the lever arm, e, above this value, it can be observed a deeper increase in the misalignment angle and, therefore, in the resultant axial deflection, $R_i\theta$.

From Figure 9 it can be observed that for an applied moment of 900 Nm (e ≅ 50.6 mm) the angular misalignment can be as high as a quarter of degree.

As already been waited for, from Figure 10 it can be observed that the partial axial deflection is symmetrical with respect to the horizontal axis (null displacement) and that the displacement is null for the balls located at $\psi = \pm 90°$.

Figure 11 shows the axial deflection, δ_a. It is observed that the axial deflection, δ_a, is approximately constant for moment values where the relationship between θ and M is approximately linear, that is, from zero up to about 600 Nm (e ≅ 33.7 mm). For higher moment values the axial deflection falls abruptly and becomes negative in the vicinity of

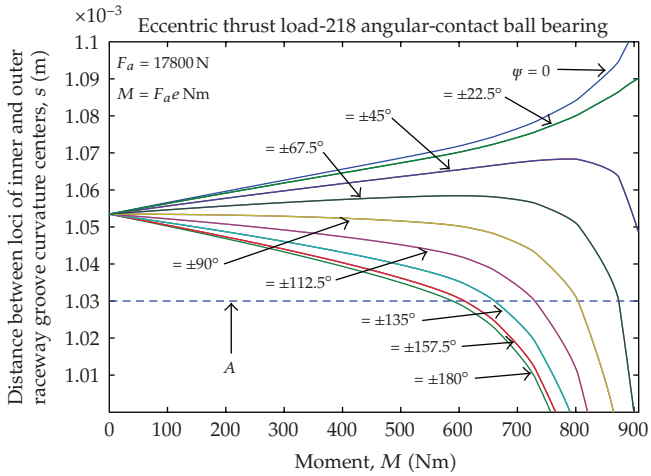

Figure 14: Distance between curvature centers, s, for 17,800 N thrust load, as a function of the Moment, M.

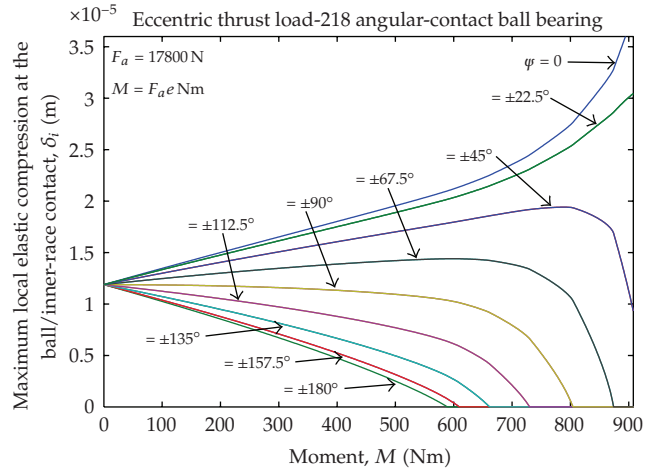

Figure 15: Maximum normal elastic compression at the ball/inner race contact, δ_i, for 17,800 N thrust load, as a function of the Moment, M.

800 Nm (e ≅ 44.9 mm). The deeper increase in θ due to the increase in the lever arm forces the decrease of δ_a to preserve the force and moment static balances.

Figure 12 shows the total axial deflection, δ_t. It can be observed that the total axial deflection, δ_t, is the axial deflection, δ_a, in two situations: under centric thrust load ($e = 0$), where all balls have the same axial deflection ($3.6011095400455 \times 10^{-5}$ m), and under eccentric thrust load for balls located at $\psi = \pm 90°$. Increasing from zero the lever arm, an almost linear increase (decrease) in the total axial deflection is observed for the balls whose angular positions satisfy $|\psi| < 90°$ ($|\psi| > 90°$). This relation is approximately linear up to vicinity of $M = 600$ Nm when the ball located at $\psi = 180°$ occurs to be unloaded, that is, $\delta_t(\psi = 180°) = 0$ for $M = 588.9687$ Nm ($e = 3.3088 \times 10^{-2}$ m).

From Figure 12 it is observed that for eccentricity of about 50 mm the total axial deflection of the most heavily loaded ball can reach one tenth of millimeter.

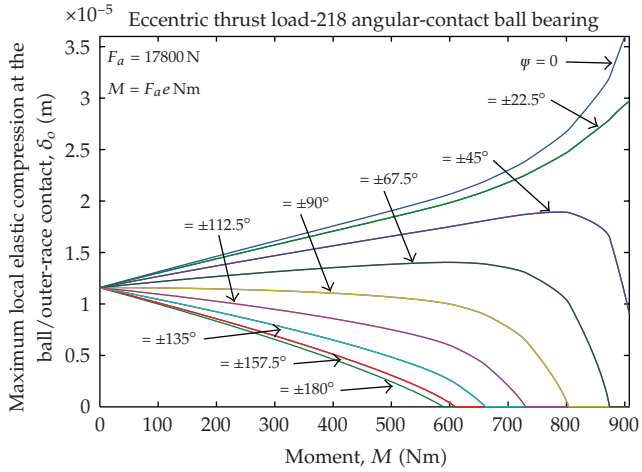

Figure 16: Maximum normal elastic compression at the ball/outer-race contact, δ_o, for 17,800 N thrust load, as a function of the Moment, M.

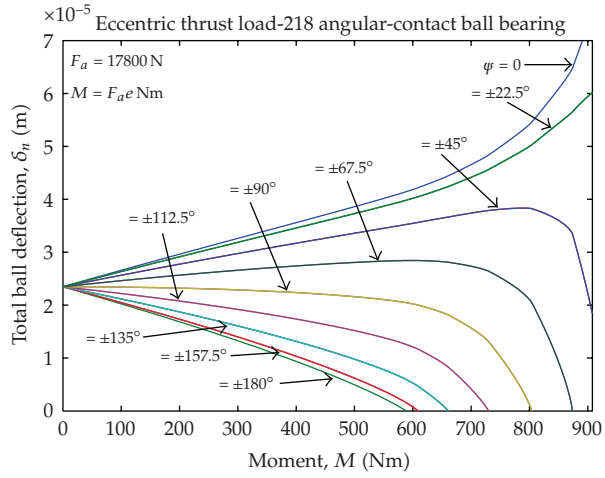

Figure 17: Total ball deflection, δ_n, for 17,800 N thrust load, as a function of the Moment, M.

The Figure 13 shows the loading zone, ψ_l. The increase of the moment above 587.4 Nm (or lever arm above 3.3×10^{-2} m) causes the decrease of the loading zone from initial value $\psi_l = \pm 180°$, with the successive unloading of the balls pairs located at $\psi = \pm 157.5°$ ($M = 609.448$ Nm), $\psi = \pm 135°$ ($M = 661.1407$ Nm), $\psi = \pm 112.5°$ ($M = 729.9584$ Nm), $\psi = \pm 90°$ ($M = 803.9741$ Nm), and $\psi = \pm 67.5°$ ($M = 873.7125$ Nm), respectively. Going ahead cause the unloading of the balls pair located at $\psi = \pm 45°$. However, it is not advisable to go beyond $M = 900$ Nm, once the radial displacements between curvature centers start to acquire micrometer order values and they cannot more be disregarded.

Figure 13 shows a substantial difference between results found in this work and those found by Harris. While Harris found a loading zone of 92.86° (p. 252) for an eccentricity of 50.8 mm, this work found a loading zone of 53.66°. Considering the last result as reference, this represents an error of +73% in the loading angle, meaning that Harris calculation has underestimated the effect of the moment M.

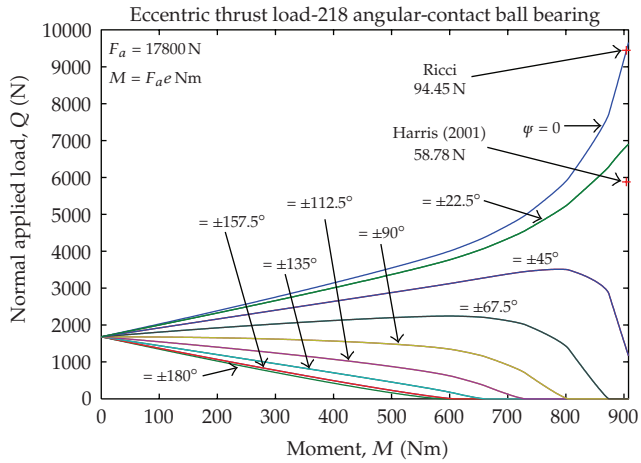

Figure 18: Normal ball load, Q, for 17,800 N thrust load, as a function of the Moment, M.

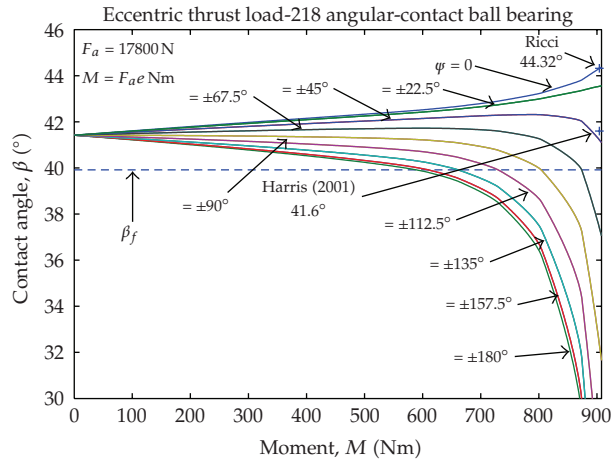

Figure 19: Contact Angle, β, for 17,800 N thrust load, as a function of the Moment, M.

Figure 14 shows the distance between loci of inner and outer raceway groove curvature centers, s. It can be observed that the distance, s, under centric thrust load ($e = 0$), is the same for all balls ($1.053468971830 \times 10^{-3}$ m). Increasing from zero the lever arm, an almost linear increase (decrease) in the distance, s, is observed for the balls whose angular positions satisfy $|\psi| < 90°$ ($|\psi| > 90°$). This relation is approximately linear up to vicinity of $M = 600$ Nm when the ball located at $\psi = 180°$ occurs to be unloaded, that is, $s(\psi = 180°) = A$ for $M = 588.9687$ Nm ($e = 3.3088 \times 10^{-2}$ m).

The increase of the moment above 588.9687 Nm (or lever arm above 3.3088×10^{-2} m) causes the decrease of the loading zone, as already explained, with the successive unloading of the ball pairs. At the points where the unloading occurs it is observed that the distance s falls below of the distance between centers of curvature, A, for the unloaded bearing.

Figures 15 and 16 show the maximum normal elastic compressions at the ball/inner-race and ball/outer-race contacts, δ_i and δ_o, respectively. It can be observed that δ_i and δ_o, under centric thrust load ($e = 0$), are the same for all balls ($1.18852986717367 \times 10^{-5}$ m for δ_i

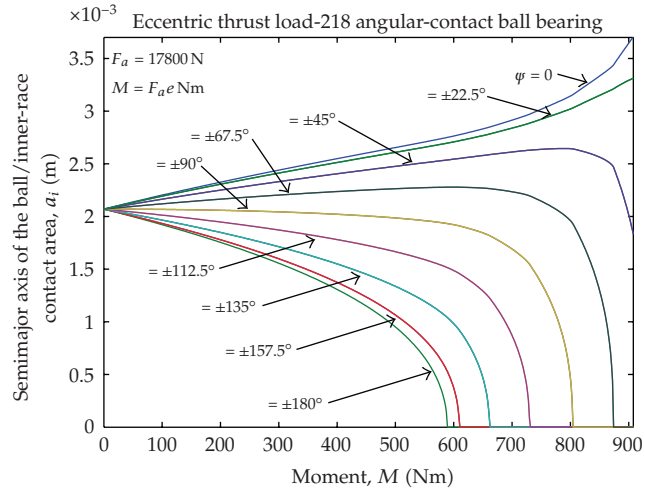

Figure 20: Semimajor axis of the ball/inner-race contact area, a_i, for 17,800 N thrust load, as a function of the Moment, M.

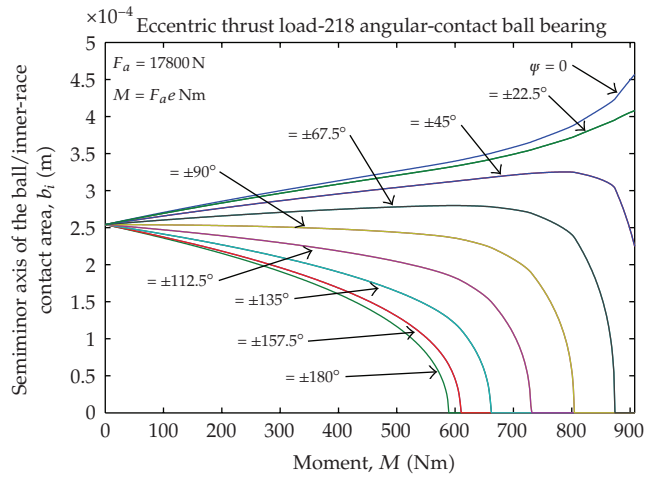

Figure 21: Semiminor axis of the ball/inner-race contact area, b_i, for 17,800 N thrust load, as a function of the Moment, M.

and $1.15836731583185 \times 10^{-5}$ m for δ_o) and that the deformation for the maximum loaded ball, in both cases, can reach values as high as 36 μm for moment about 900 Nm.

Figure 17 shows the total normal ball deflection, δ_n, that can be obtained by summing the maximum normal elastic compressions on the inner and outer races, δ_i and δ_o, or by subtracting A from s, once $\delta_n = s - A > 0$ also. It can be observed that δ_n, under centric thrust load ($e = 0$), is the same for all balls ($2.3468971830055 \times 10^{-5}$ m) and that the total normal elastic deformation for the maximum loaded ball can reach values as high as 70 μm for moment about 900 Nm.

Figure 18 shows the normal ball load, Q. It can be observed that the normal ball load, Q, under centric thrust load ($e = 0$), is the same for all balls (1, 681.663561507042 N). Increasing from zero the lever arm, an almost linear increase (decrease) in the normal ball

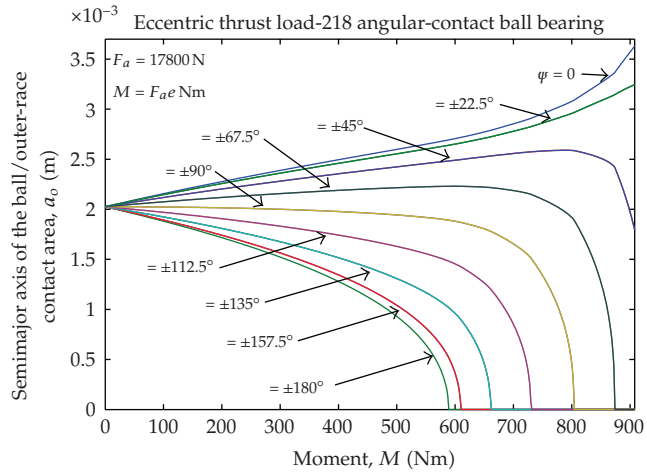

Figure 22: Semimajor axis of the ball/outer-race contact area, a_o, for 17,800 N thrust load, as a function of the Moment, M.

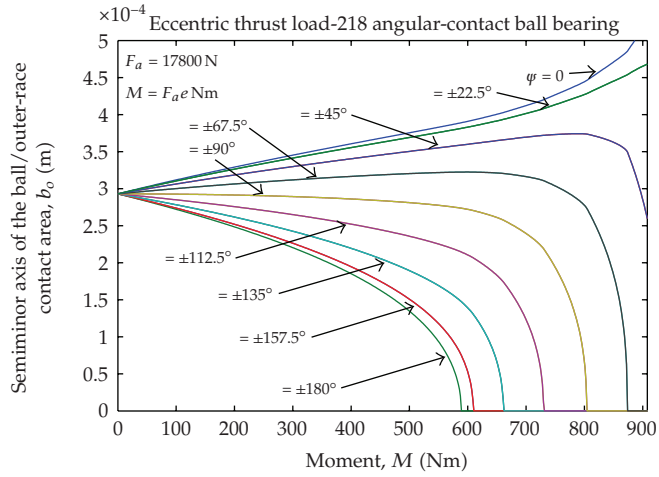

Figure 23: Semiminor axis of the ball/outer-race contact area, b_o, for 17,800 N thrust load, as a function of the Moment, M.

load is observed for the balls whose angular positions satisfy $|\psi| < 90°$ ($|\psi| > 90°$). This relation is approximately linear up to vicinity of $M = 600$ Nm when the ball located at $\psi = 180°$ occurs to be unloaded, that is, $Q(\psi = 180°) = 0$ for $M = 589.18$ Nm ($e = 3.31 \times 10^{-2}$ m).

Figure 18, as well as Figure 13, shows a substantial difference between results found in this work and those found by Harris. While Harris found a 5, 878 N magnitude for the maximum normal ball load (p. 252), for an applied load eccentricity of 50.8 mm, this work found a 9, 445 N maximum normal ball load. This represents an error of −62.2% in the normal load, meaning that the Harris calculation has underestimated the normal load for the maximum loaded ball.

Figure 19 shows the contact angle, β. It can be observed that the contact angle, β, under centric thrust load ($e = 0$), is the same for all balls (41.417986227161386^o). Increasing from zero the lever arm, an almost linear increase (decrease) in the contact angle is observed for

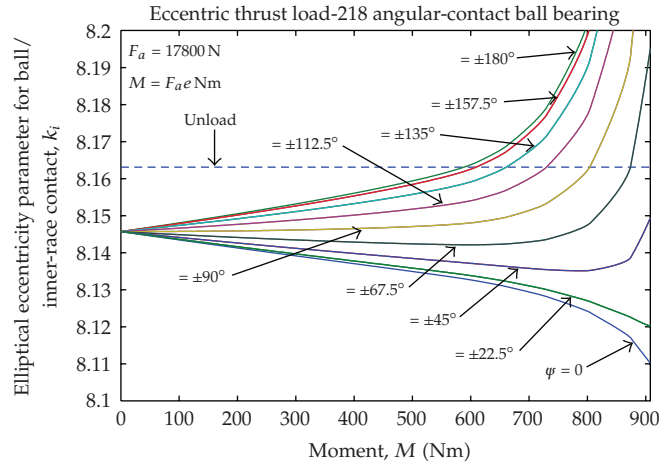

Figure 24: Elliptical eccentricity parameter for ball/inner-race contact, k_i, for 17,800 N thrust load, as a function of the Moment, M.

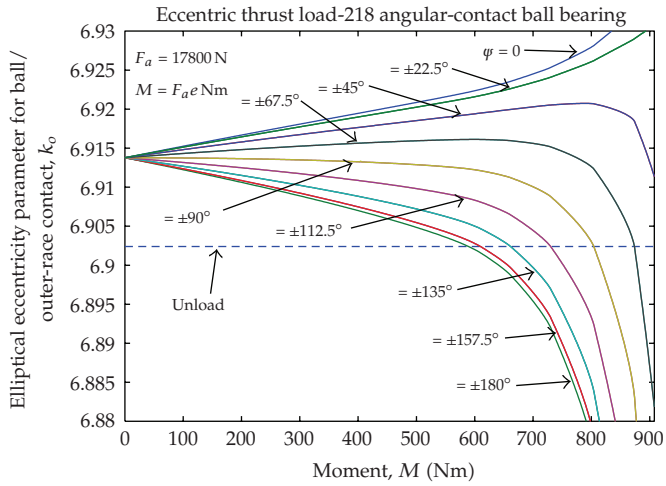

Figure 25: Elliptical eccentricity parameter for ball/outer-race contact, k_o, for 17,800 N thrust load, as a function of the Moment, M.

the balls whose angular positions satisfy $|\psi| < 90°$ ($|\psi| > 90°$). This relation is approximately linear up to vicinity of $M = 600$ Nm when the ball located at $\psi = 180°$ occurs to be unloaded, that is, $\beta(\psi = 180°) = \beta_f$ for $M = 589.18$ Nm ($e = 33.1$ mm).

Figure 19, as well as Figure 18 and Figure 13, shows a substantial difference between results found in this work and to those found by Harris. While Harris has assumed a contact angle magnitude of 41.6^o for all balls (p. 252), under a 50.8 mm applied load eccentricity, contact angles ranging from 44.31727851159821^o to 16.16919216282055^o were found in this work while ψ were varied from $\psi = 0°$ to $\pm 180^o$, respectively. This represents errors between −6.1% and +157.3% in the contact angles determination, meaning that the Harris calculation has underestimated (strongly overestimated) the contact angles for balls located at angular positions satisfying $|\psi| < 45°$($|\psi| > 45°$).

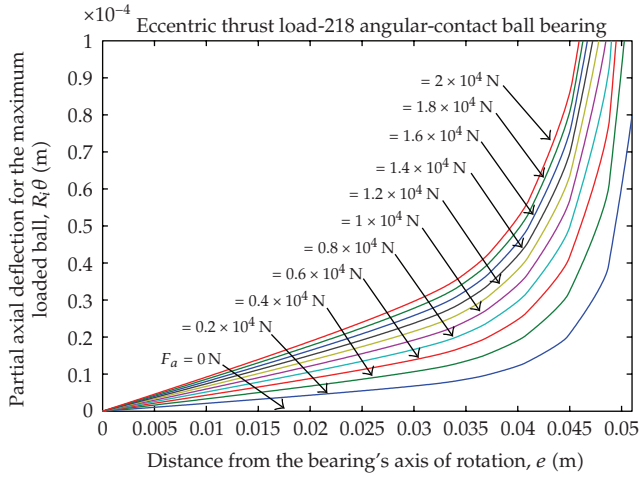

Figure 26: Partial axial displacement for the maximum loaded ball, $R_i\theta$, as a function of lever arm, e.

Figures 20 and 22 show the semimajor axes of the ball/inner-race and ball/outer-race contact areas, a_i and a_o, respectively. It can be observed that a_i and a_o, under centric thrust load ($e = 0$), are the same for all balls (2.069901480072 mm for a_i and 2.025827993682 mm for a_o) and that the major axes for the maximum loaded ball, in both cases, can reach values as high as 7.4 mm for moment about 900 Nm.

Figures 21 and 23 show the semiminor axes of the ball/inner-race and ball/outer-race contact areas, b_i and b_o, respectively. It can be observed that b_i and b_o, under centric thrust load ($e = 0$), are the same for all balls (0.254108993896064 mm for b_i and 0.293013306181356 mm for b_o) and that the major axes for the maximum loaded ball, in both cases, can reach values as high as 0.9 mm for moment about 900 Nm.

Figures 24 and 25 show the elliptical eccentricity parameters for ball/inner-race and ball/outer-race contact, k_i and k_o, respectively. It can be observed that k_i and k_o, under centric thrust load ($e = 0$), are the same for all balls (8.1457 for k_i and 6.9138 for k_o). Increasing from zero the lever arm, an almost linear increase (decrease) in the parameter k_i is observed for the balls whose angular positions satisfy $|\psi| > 90^\circ$ ($|\psi| < 90^\circ$), and an almost linear increase (decrease) in the parameter k_o is observed for the balls whose angular positions satisfy $|\psi| < 90^\circ$ ($|\psi| > 90^\circ$). These relations are approximately linear up to vicinity of $M = 600$ Nm when the ball located at $\psi = 180^\circ$ occurs to be unloaded. It can be observed that $k_i(\psi = 180^\circ) \cong 8.1631$ and $k_o(\psi = 180^\circ) \cong 6.9024$ when $M = 588.9687$ Nm ($e = 3.3088 \times 10^{-2}$ m).

The increase of the moment above 588.9687 Nm (or lever arm above 3.3088×10^{-2} m), causes the successive unloading of the ball pairs. At the points where the unloading occurs the values of the parameters k_i and k_o remain roughly equal to those indicated in the preceding paragraph for $\psi = 180^\circ$. So, it can be observed that the contact ellipse of the inner race is slightly more eccentric than that of the contact ellipse of the outer race. For $M = 900$ Nm, for example, while k_i varies numerically from 8.11, for the most heavily loaded ball, to 8.37, for the minimum loaded ball, k_o varies from 6.83 to 6.37, respectively.

5.2. Numerical Results for Thrust Load Ranging from 0 up to 20,000 N

Graphics for various thrust loads also are shown. The following graphics present curves for thrust loads ranging from 0 up to 20, 000 N as functions of lever arm, e:

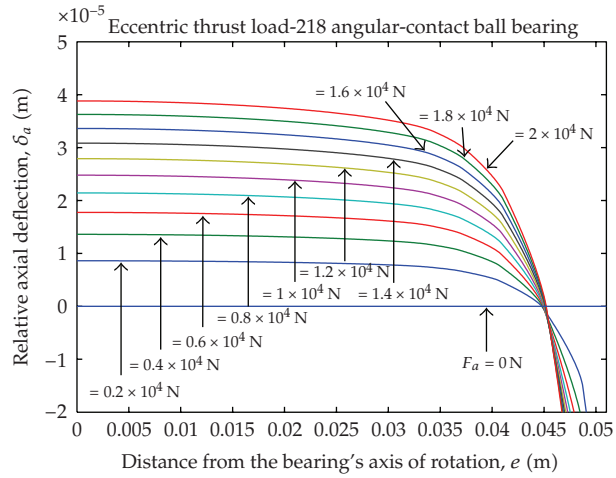

Figure 27: Relative axial displacement, δ_a, as a function of lever arm, e.

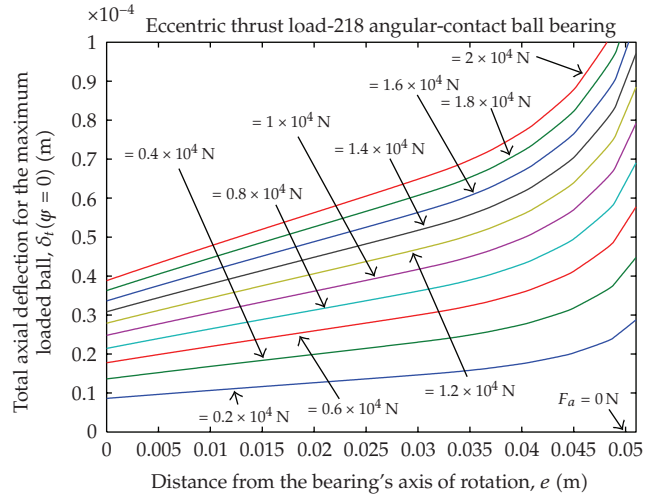

Figure 28: Total relative axial deflection for the maximum loaded ball, $\delta_t(\psi = 0)$, as a function of lever arm, e.

(i) partial axial displacement for the maximum loaded ball, $R_i\theta$ (Figure 26),

(ii) relative axial displacement, δ_a (Figure 27),

(iii) total relative axial deflection for the maximum loaded ball, $\delta_t(\psi = 0)$ (Figure 28),

(iv) total relative axial deflection for the minimum loaded ball, $\delta_t(\psi = 180°)$ (Figure 29),

(v) loading zone, ψ_l (Figure 30),

(vi) distance between loci of inner and outer raceway groove curvature centers for the maximum loaded ball, $s(\psi = 0)$ (Figure 31),

(vii) distance between loci of inner and outer raceway groove curvature centers for the minimum loaded ball, $s(\psi = 180°)$ (Figure 32),

(viii) total normal ball deflection for the maximum loaded ball, $\delta_n(\psi = 0)$ (Figure 33),

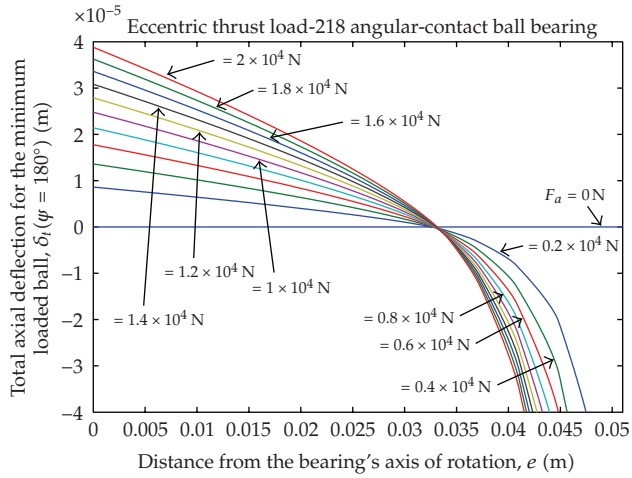

Figure 29: Total relative axial deflection for the minimum loaded ball, $\delta_t(\psi = 180°)$, as a function of lever arm, e.

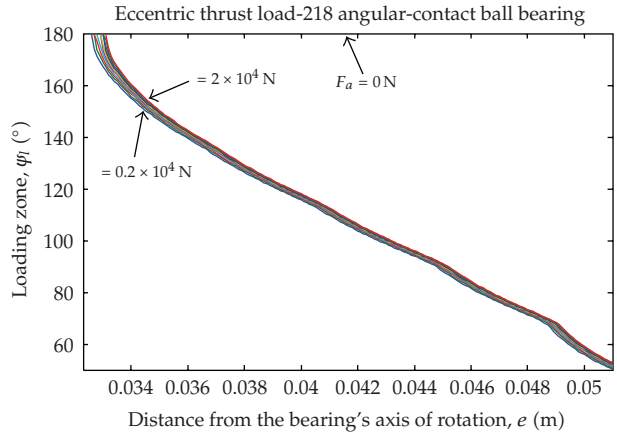

Figure 30: Loading zone, ψ_l, as a function of lever arm, e.

(ix) total normal ball deflection for the minimum loaded ball, $\delta_n(\psi = 180°)$ (Figure 34),

(x) ball-raceway normal load for the maximum loaded ball, $Q(\psi = 0)$ (Figure 35),

(xi) ball-raceway normal load for the minimum loaded ball, $Q(\psi = 180°)$ (Figure 36),

(xii) contact angle for the maximum loaded ball, $\beta(\psi = 0)$ (Figure 37),

(xiii) contact angle for the minimum loaded ball, $\beta(\psi = 180°)$ (Figure 38),

(xiv) semimajor axis of the ball/inner-race contact area for the maximum loaded ball, $a_i(\psi = 0)$ (Figure 39),

(xv) semiminor axis of the ball/inner-race contact area for the maximum loaded ball, $b_i(\psi = 0)$ (Figure 40),

(xvi) semimajor axis of the ball/outer-race contact area for the maximum loaded ball, $a_o(\psi = 0)$ (Figure 41),

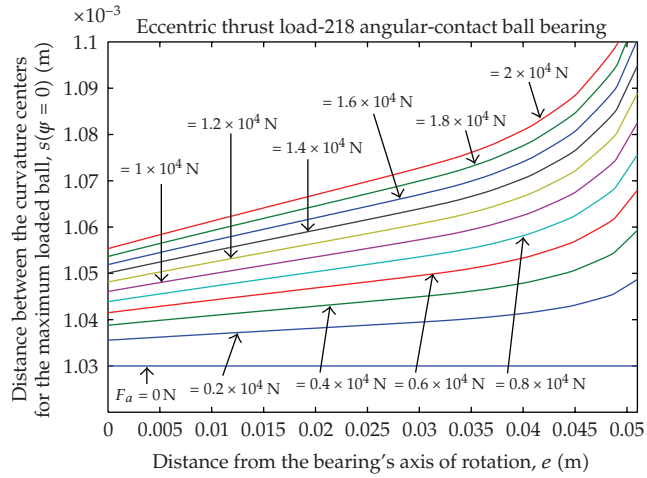

Figure 31: Distance between loci of inner and outer raceway groove curvature centers for the maximum loaded ball, $s(\psi = 0)$, as a function of lever arm, e.

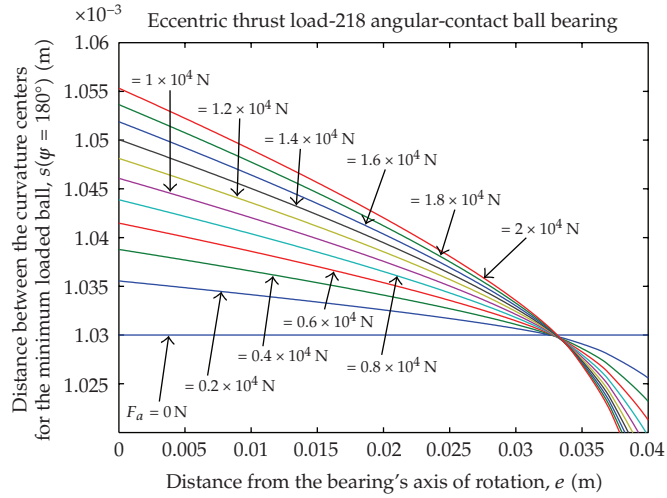

Figure 32: Distance between loci of inner and outer raceway groove curvature centers for the minimum loaded ball, $s(\psi = 180°)$, as a function of lever arm, e.

(xvii) semiminor axis of the ball/outer-race contact area for the maximum loaded ball, $b_o(\psi = 0)$ (Figure 42),

(xviii) semimajor axis of the ball/inner-race contact area for the minimum loaded ball, $a_i(\psi = 180°)$ (Figure 43),

(xix) semiminor axis of the ball/inner-race contact area for the minimum loaded ball, $b_i(\psi = 180°)$ (Figure 44),

(xx) semimajor axis of the ball/inner-race contact area for the minimum loaded ball, $a_o(\psi = 180°)$ (Figure 45),

(xxi) semiminor axis of the ball/inner-race contact area for the minimum loaded ball, $b_o(\psi = 180°)$ (Figure 46),

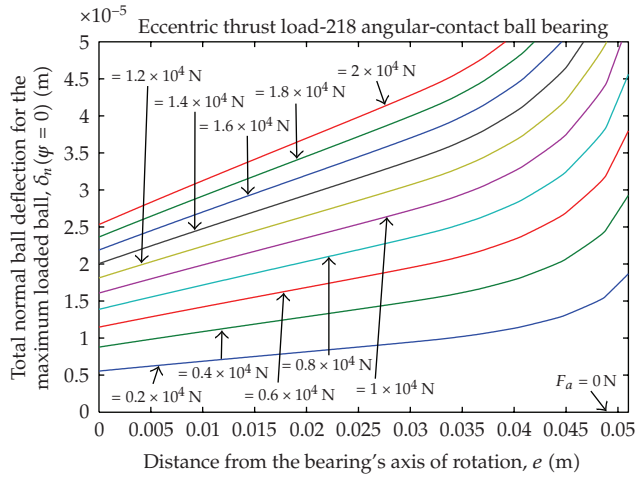

Figure 33: Total normal ball deflection for the maximum loaded ball, $\delta_n(\psi = 0)$, as a function of lever arm, e.

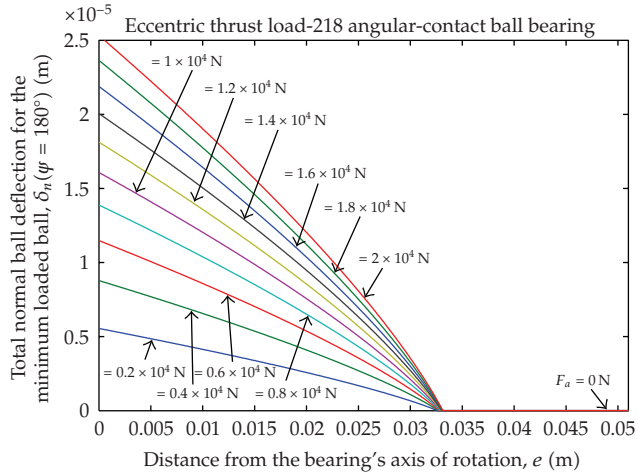

Figure 34: Total normal ball deflection for the minimum loaded ball, $\delta_n(\psi = 180°)$, as a function of lever arm, e.

(xxii) elliptical eccentricity parameter of the ball/inner-race contact area for the maximum loaded ball, $k_i(\psi = 0)$ (Figure 47),

(xxiii) elliptical eccentricity parameter of the ball/outer-race contact area for the maximum loaded ball, $k_o(\psi = 0)$ (Figure 48),

(xxiv) elliptical eccentricity parameter of the ball/inner-race contact area for the minimum loaded ball, $k_i(\psi = 180°)$ (Figure 49),

(xxv) elliptical eccentricity parameter of the ball/outer-race contact area for the minimum loaded ball, $k_o(\psi = 180°)$ (Figure 50).

Due to the size quite extensive of the paper comments about the figures will be omitted from now on.

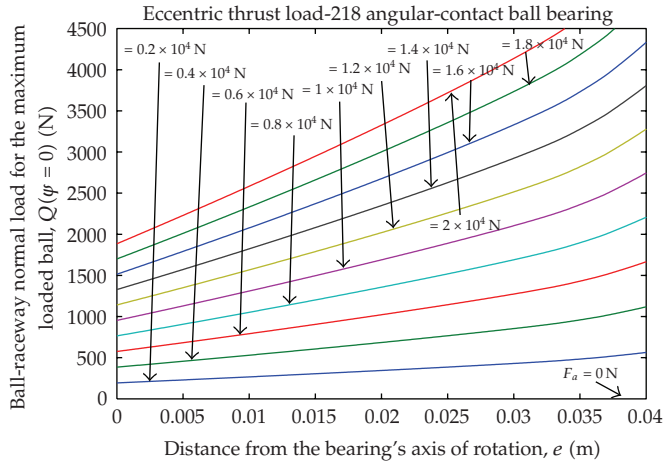

Figure 35: Ball-raceway normal load for the maximum loaded ball, $Q(\psi = 0)$, as a function of lever arm, e.

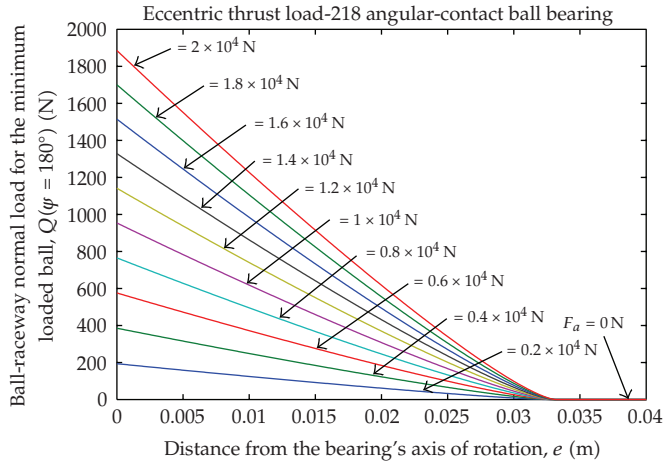

Figure 36: Ball-raceway normal load for the minimum loaded ball, $Q(\psi = 180°)$, as a function of lever arm, e.

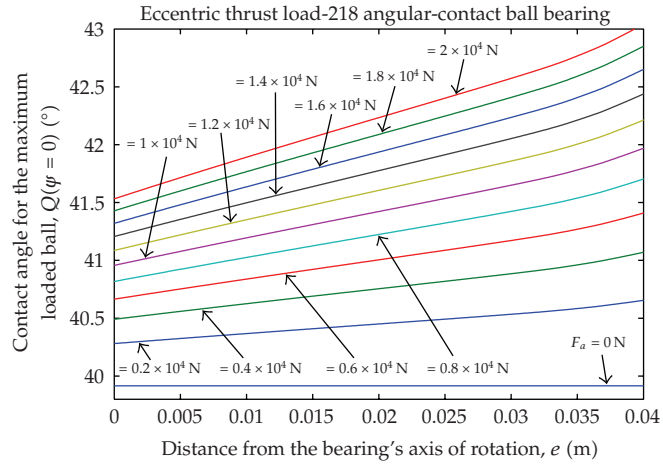

Figure 37: Contact angle for the maximum loaded ball, $\beta(\psi = 0)$, as a function of lever arm, e.

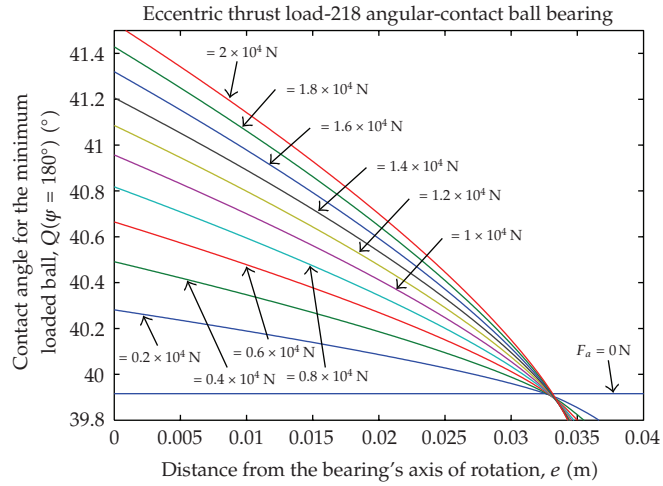

Figure 38: Contact angle for the minimum loaded ball, $\beta(\psi = 180°)$, as a function of lever arm, e.

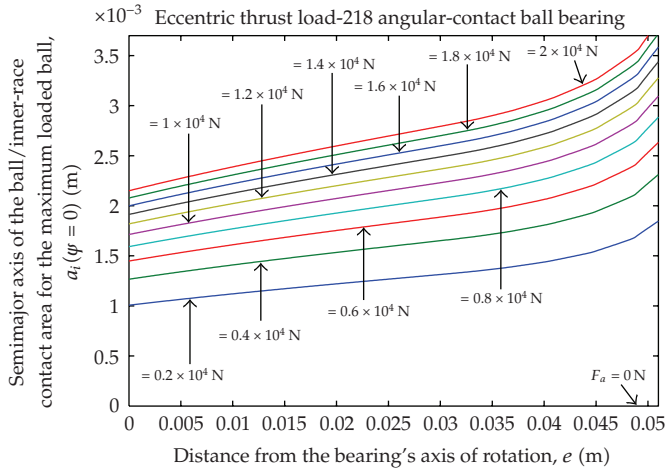

Figure 39: Semimajor axis of the ball/inner-race contact area for the maximum loaded ball, $a_i(\psi = 0)$, as a function of lever arm, e.

6. Conclusions

The importance of this work lies in the fact that it uses a new procedure for gettinnng numerically, accurately, and quickly the static load distribution of a single-row, angular-contact ball bearings, subjected to a known thrust load which is applied to a variable distance from the geometric bearing center line. Precise applications, as for example, space applications, require a precise determination of the static loading. Models available in literature are approximate and often are not compatible with the desired degree of accuracy. This work can be extended to determine the loading on high-speed bearings where centrifugal and gyroscopic forces are not discarded. The results of this work can be used in the accurate determination of the friction torque of the ball bearings, under any operating condition of temperature and speed.

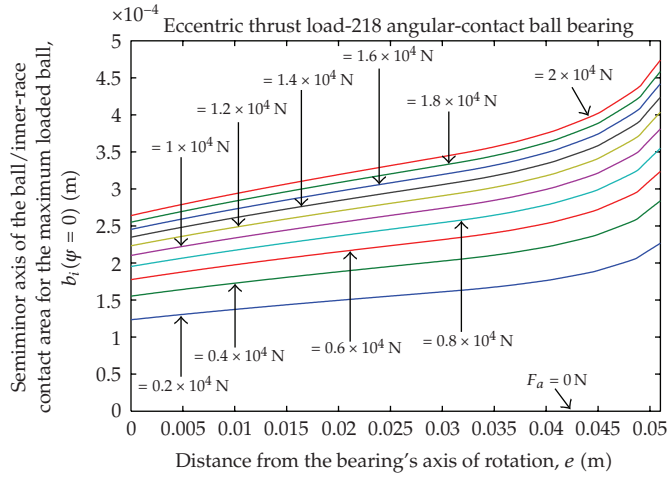

Figure 40: Semiminor axis of the ball/inner-race contact area for the maximum loaded ball, $b_i(\psi = 0)$, as a function of lever arm, e.

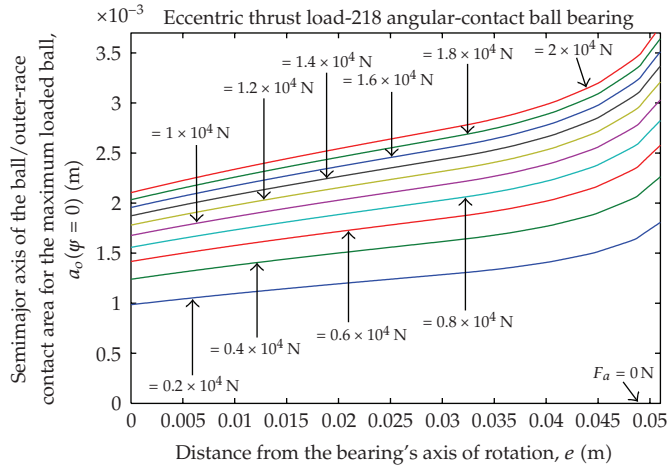

Figure 41: Semimajor axis of the ball/outer-race contact area for the maximum loaded ball, $a_o(\psi = 0)$, as a function of lever arm, e.

Symbols

a: Semimajor axis of the projected contact, m
A: Distance between raceway groove curvature centers, m
b: Semiminor axis of the projected contact, m
B: $f_o + f_i - 1$, total curvature
d: Raceway diameter, m
d_a: Bearing outer diameter, m
d_b: Bearing inner diameter, m
d_c: Contact diameter, m
d_e: Bearing pitch diameter, m
D: Ball diameter, m

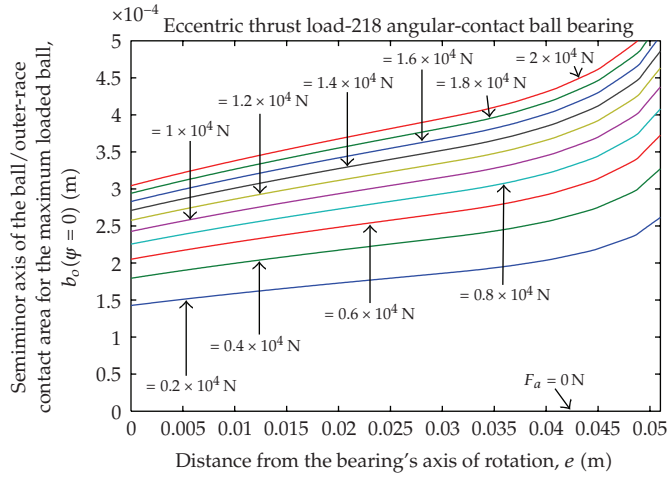

Figure 42: Semiminor axis of the ball/outer-race contact area for the maximum loaded ball, $b_o(\psi{=}0)$, as a function of lever arm, e.

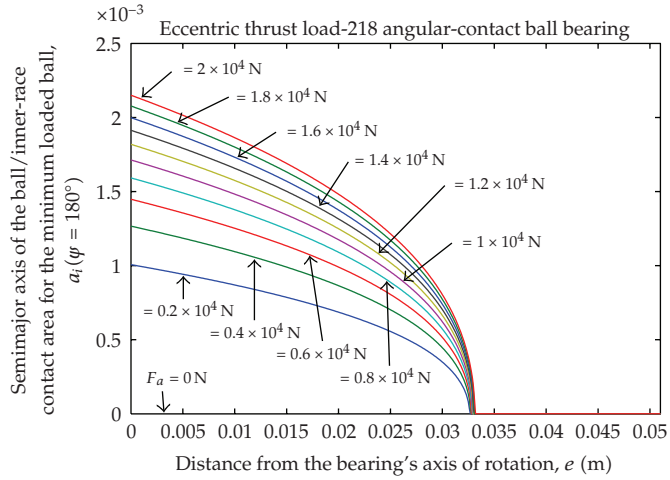

Figure 43: Semimajor axis of the ball/inner-race contact area for the minimum loaded ball, $a_i(\psi = 180°)$, as a function of lever arm, e.

e: Eccentricity of loading, m
E: Modulus of elasticity, N/m^2
E': Effective elastic modulus, N/m^2
$\mathbf{E}$: Elliptic integral of second kind
f: Raceway groove radius $\div D$
F: Applied load, N
k: a/b
K: Load-deflection factor, N/m$^{3/2}$
$\mathbf{K}$: Elliptic integral of first kind
M: eF_a
P_d: Diametral clearance, m
P_e: Free endplay, m

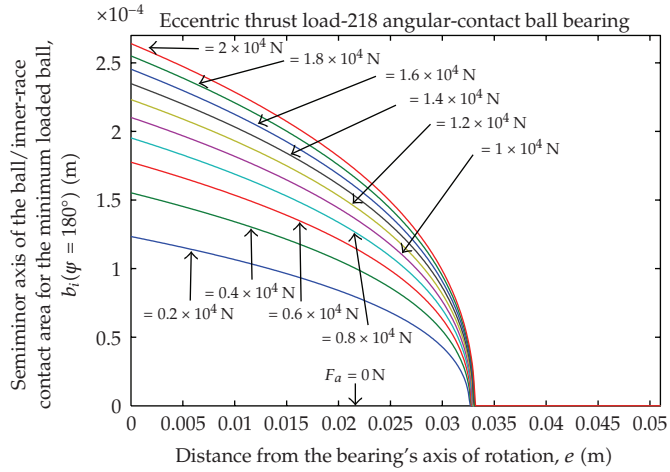

Figure 44: Semiminor axis of the ball/inner-race contact area for the minimum loaded ball, $b_i(\psi = 180°)$, as a function of lever arm, e.

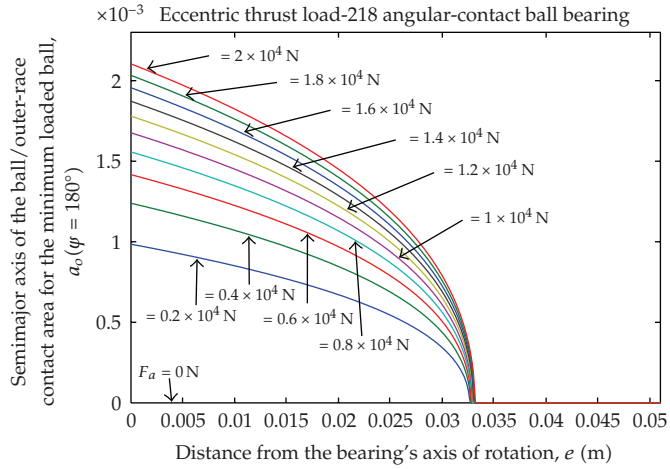

Figure 45: Semimajor axis of the ball/outer-race contact area for the minimum loaded ball, $a_o(\psi = 180°)$, as a function of lever arm, e.

Q: Ball-raceway normal load, N
r: Raceway groove curvature radius, solids curvature radius, m
s: Distance between loci of inner and outer raceway groove curvature centers, m
R: Curvature radius, radius of locus of raceway groove curvature centers, m
Z: Number of rolling elements
β: Contact angle, rad, ^{o}
β_f: Free-contact angle, rad, ^{o}
γ: $D \cos \beta / d_e$
Γ: Curvature difference
δ: Deflection or contact deformation, m
$\Delta\psi$: Angular spacing between rolling elements, rad, ^{o}
ε: Load distribution factor

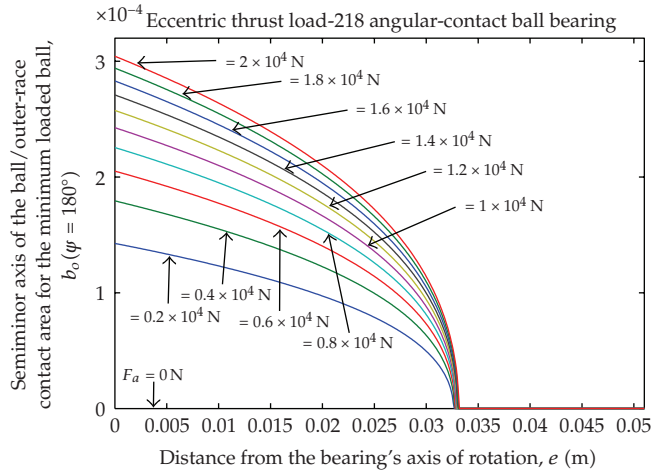

Figure 46: Semiminor axis of the ball/outer-race contact area for the minimum loaded ball, $b_o(\psi = 180°)$, as a function of lever arm, e.

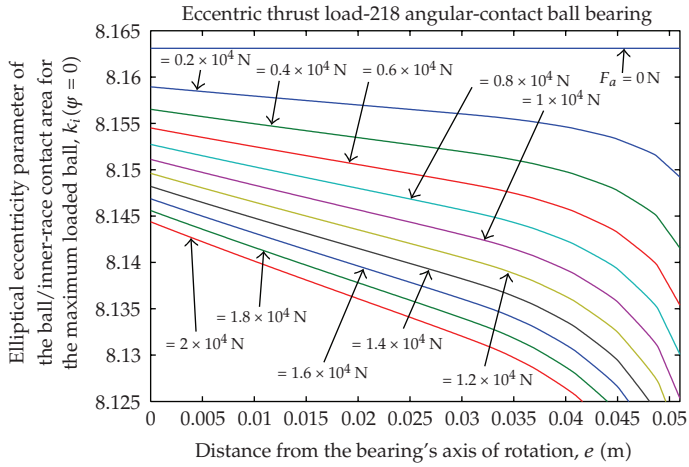

Figure 47: Elliptical eccentricity parameter of the ball/inner-race contact area for the maximum loaded ball, $k_i(\psi = 0)$, as a function of lever arm, e.

θ: Bearing misalignment angle, rad, ^{o}
υ: Poisson's ratio
φ: Auxiliary angle
ψ: Azimuth angle, rad, $^\circ$.

Subscripts:

a refers to solid a or axial direction.
b refers to solid b.
x, y refers to coordinate system.
i refers to inner raceway.

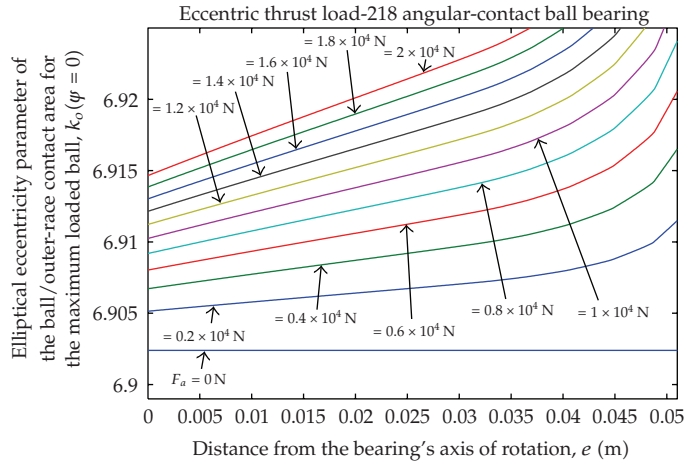

Figure 48: Elliptical eccentricity parameter of the ball/outer-race contact area for the maximum loaded ball, $k_o(\psi = 0)$, as a function of lever arm, e.

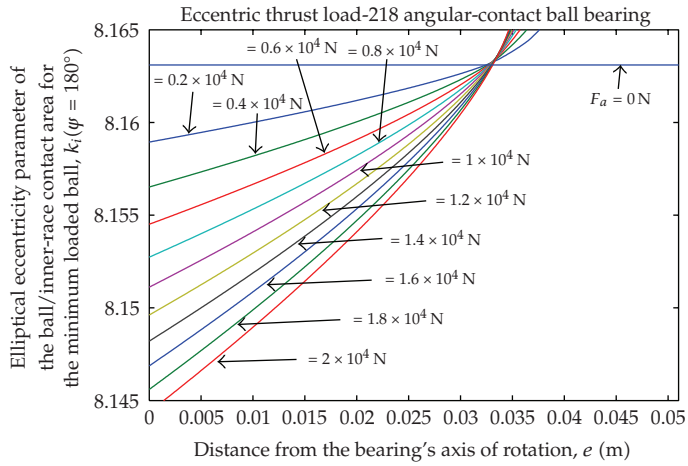

Figure 49: Elliptical eccentricity parameter of the ball/inner-race contact area for the minimum loaded ball, $k_i(\psi = 180°)$, as a function of lever arm, e.

j refers to rolling-element position.
n refers to direction collinear with normal load, integer number.
o refers to outer raceway.
t refers to total axial deformation.

Acknowledgments

The author thanks the financial support provided by the Brazilian Institute for Space Research (INPE), the Brazilian Scientific and Technological Development Council (CNPq), The State of

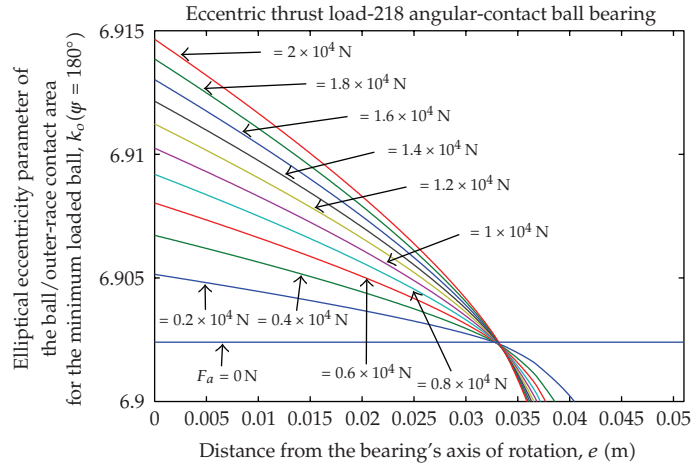

Figure 50: Elliptical eccentricity parameter of the ball/outer-race contact area for the minimum loaded ball, $k_o(\psi = 180°)$, as a function of lever arm, e.

São Paulo Research (FAPESP), and The Coordination of Development of Higher-Level Staff (CAPES). And the author thanks also José Pelógia da Silva for doing Figures 2 up to 7.

References

[1] R. Stribeck, "Ball bearings for various loads," *Transactions of the ASME*, vol. 29, pp. 420–463, 1907.
[2] H. Sjoväll, "The load distribution within ball and roller bearings under given external radial and axial load," *Teknisk Tidskrift, Mekaniska*, p. 9, 1933.
[3] A. Jones, *Analysis of Stresses and Deflections*, New Departure Engineering Data, Bristol, Conn, USA, 1946.
[4] J. Rumbarger, "Thrust bearings with eccentric loads," *Machine Design*, 1962.
[5] T. Harris, *Rolling Bearing Analysis*, John Wiley & Sons, New York, NY, USA, 4th edition, 2001.
[6] M. C. Ricci, "Ball bearings subjected to a variable eccentric thrust load," in *Booklet of Abstracts of the 8th Brazilian Conference on Dynamics, Control and Applications (DINCON '09)*, Bauru, Brazil, May 2009.
[7] M. C. Ricci, "Ball bearings subjected to a variable eccentric thrust load," in *Proceedings of the 8th Brazilian Conference on Dynamics, Control and Applications (DINCON '09)*, Bauru, Brazil, May 2009.
[8] M. C. Ricci, "Internal loading distribution in statically loaded ball bearings," in *Program and Abstracts of the 1st International Conference on Computational Contact Mechanics (ICCCM '09)*, pp. 21–22, Lecce, Italy, September 2009.
[9] M. C. Ricci, "Internal loading distribution in statically loaded ball bearings subjected to a combined radial and thrust load, including the effects of temperature and fit," in *Proceedings of World Academy of Science, Engineering and Technology (WCSET '09)*, vol. 57, Amsterdam, The Netherlands, September 2009.
[10] M. C. Ricci, "Internal loading distribution in statically loaded ball bearings subjected to a combined radial and thrust load," in *Book of Abstracts of the 6th International Congress of Croatian Society of Mechanics (ICCSM '09)*, p. 163, Dubrovnik, Croatia, September 2009.
[11] M. C. Ricci, "Internal loading distribution in statically loaded ball bearings subjected to a combined radial and thrust load," in *Proceedings of the 6th International Congress of Croatian Society of Mechanics (ICCSM '09)*, Dubrovnik, Croatia, September 2009.
[12] M. C. Ricci, "Internal loading distribution in statically loaded ball bearings subjected to a combined radial, thrust, and moment load," in *Abstracts of the 60th International Astronautical Congress*, Daejeon, South Korea, October 2009.
[13] M. C. Ricci, "Internal loading distribution in statically loaded ball bearings subjected to a combined radial, thrust, and moment load," in *Proceedings of the 60th International Astronautical Congress*, p. 163, Daejeon, South Korea, October 2009.

[14] M. C. Ricci, "Internal loading distribution in statically loaded ball bearings subjected to a combined radial, thrust, and moment load, including the effects of temperature and fit," in *Proceedings of the 11th Pan-American Congress of Applied Mechanics*, Foz do Iguaçu, Brazil, January 2010.
[15] B. J. Hamrock and W. J. Anderson, "Arched-outer-race ball-bearing considering centrifugal forces," NASA Report TN D-6765, NASA, Moffett Field, Calif, USA, 1972.
[16] H. Hertz, *On the contact of elastic solids and on hardness, in: D.E. Jones, G.A. Schott (Eds.)*, Miscellaneous Papers by Heinrich Hertz, Macmillan, London, 1896.
[17] B. J. Hamrock and W. J. Anderson, "Rolling-element bearings," NASA Report RP 1105, NASA, Moffett Field, Calif, USA, 1983.